MUSIC Imaging and Electromagnetic Inverse Scattering of Multiple-Scattering Small Anisotropic Spheres

Yu Zhong and Xudong Chen

***Abstract*—The Foldy-Lax equation is used to derive a multiple scattering model for the multiple-scattering small anisotropic spheres. By this model, if the number of the non-zero singular values of the multistatic response (MSR) matrix is smaller than the number of the antennas, the range space of the MSR matrix is found to be spanned by the background Green's function vectors corresponding to the x, y and z components of the electric and magnetic dipoles induced in each scatterer, which indicates that the multiple signal classification (MUSIC) method could be implemented to obtain the locations of the scatterers. After estimating the positions of the scatterers, a non-iterative analytical method is proposed for retrieving the polarization strength tensors as well as the orientations of the principle axes of each scatterer. Two numerical simulations show that, the MUSIC method and the non-iterative method are efficacious for the nonlinear inverse scattering problem of determining the locations and polarization strength tensors of multiple-scattering small anisotropic spheres. Such methods could also be applied to the inversion of small isotropic spheres or extended to the inversion of small bianisotropic spheres.**

***Index Terms*—Inverse scattering problems, linear methods, multiple scattering, small anisotropic spheres.**

I. Introduction

THE imaging methods for small inclusions based on the decomposition of the so called multistatic response (MSR) matrix [1] have been of great interest for many years, which may be due to its potential applications in many areas, such as geophysics, nondestructive testing and evaluation, biological studies at cell level, and modeling in medicine. Among these methods, there are two that have been intensively discussed in acoustics and electromagnetics, namely, the eigenvalue decomposition of time-reversal operator (DORT) [1]–[3], and the multiple signal classification (MUSIC) [1], [4]–[6], [17]. As mentioned in [1] and [2], for the time-harmonic illumination, in order to obtain a good image, the small multiple scatterers need to be well-resolved, i.e., the electromagnetic fields scattered from any one of the scatterers, upon time reversing (back propagation) at the receivers, produce null fields at the other scatterers. It has been shown in [1], [2] and [4] that, under such a condition, a one-to-one mapping between the individual scatterers and the singular vectors associated to the non-zero singular values of the MSR matrix could be constructed when the dimension of the MSR matrix is larger than the number of the scatterers, and any singular vector associated to a non-zero singular value is the normalized background Green's function vector evaluated at the position of its corresponding scatterer. Therefore, due to the orthogonality between the singular vectors of the MSR matrix, a singular vector associated to a non-zero singular value could be used to locate its corresponding scatterer without generating disturbance to the image of the other scatterers, and the associated singular value also determines the corresponding scattering strength. Nevertheless, the scatterers are usually not well-resolved, and the singular vectors of the MSR matrix are the linear combinations of the background Green's function vectors evaluated at the positions of all scatterers. For the non-resolved case, the MUSIC method is a good candidate proposed to locate the small scatterers both in acoustic [4], [5] and electromagnetic [6] inverse scattering problems. As a special case of the linear sampling method, the MUSIC method is designed for the finite dimensional scattering operator [5], which is applied for point like scatterers. Unlike the DORT method, the MUSIC method uses the left null space of the MSR matrix, and it applies no matter the scatterers are well-resolved or not.

As an early attempt to implement the MUSIC method in electromagnetic inverse problems in [6], single scattering model is adopted for the well-separated small isotropic inclusions, and an approximate model is proposed for the closely spaced small isotropic inclusions, where two equivalent ellipsoids are constructed. The purposes of this paper are two folds. First, by using the Foldy-Lax equation, we derive the multiple scattering model for the small anisotropic spherical scatterers whose principle elements of the permittivity and permeability tensors are different from the background homogeneous medium's permittivity and permeability, respectively, based on which the MUSIC method is implemented to obtain the positions of the scatterers. Second, the non-linear problem of retrieving the polarization strength tensors and the orientations of the principle axes of each scatterer is tackled by a non-iterative analytical method. The proposed methods are tested through two numerical simulations. The first simulation is the far-field imaging and the retrieval of the polarization strength tensors of the well-separated scatterers, while the second one is the near-field imaging and the retrieval of the polarization strength tensors of the scatterers that are close to each other, and the latter shows that the multiple scattering

Manuscript received May 11, 2007; revised August 10, 2007. This work was supported by the Ministry of Education (Singapore) under Grants R263000357112 and R263000357133.

The authors are with the Department of Electrical and Computer Engineering, National University of Singapore, 117576 Singapore, Singapore (e-mail: zhongyu@nus.edu.sg; elechenx@nus.edu.sg).

Digital Object Identifier 10.1109/TAP.2007.910488

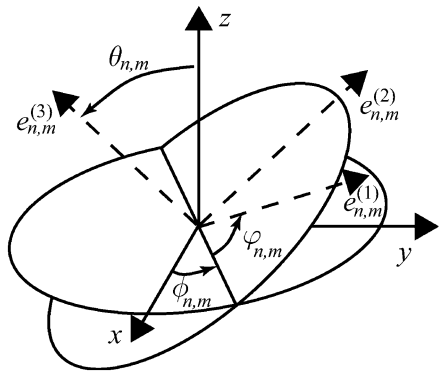

Fig. 1. The definition of the rotation angles $\phi_{n,m}, \theta_{n,m}$ and $\varphi_{n,m}$, where $e^{(l)}_{n,m}$ is the lth electric ($n = E$) or magnetic ($n = H$) principle axis of the mth scatterer, $l = 1, 2, 3$ and $m = 1, 2, \ldots, M$.

effect (MSE) cannot be ignored in order to obtain an accurate estimate of the polarization strength tensors.

II. Formulas for the Forward Problem of the Multiple-Scattering Small Anisotropic Spheres

First, we assume that N antenna units as transceivers are located at $\bar{r}_1^{'}, \bar{r}_2^{'}, \ldots, \bar{r}_N^{'}$, each of which consists of 3 small dipole antennas oriented in the x, y and z direction with length d_{ix}, d_{iy}, d_{iz} and driving current I_{ix}, I_{iy}, I_{iz}, respectively, $i = 1, 2, \ldots, N$. We also assume that M small anisotropic spherical scatterers with radii a_m are located at $\bar{r}_m, m = 1, 2, \ldots, M$. The permittivity and permeability tensors of spheres are given by

$$\bar{\bar{\epsilon}}_m = \begin{bmatrix} \epsilon_m^{xx} & \epsilon_m^{xy} & \epsilon_m^{xz} \\ \epsilon_m^{yx} & \epsilon_m^{yy} & \epsilon_m^{yz} \\ \epsilon_m^{zx} & \epsilon_m^{zy} & \epsilon_m^{zz} \end{bmatrix} = \bar{\bar{\Xi}}_{E,m}^{-1} \cdot \begin{bmatrix} \epsilon_m^{(1)} & 0 & 0 \\ 0 & \epsilon_m^{(2)} & 0 \\ 0 & 0 & \epsilon_m^{(3)} \end{bmatrix} \cdot \bar{\bar{\Xi}}_{E,m} \tag{1a}$$

and

$$\bar{\bar{\mu}}_m = \begin{bmatrix} \mu_m^{xx} & \mu_m^{xy} & \mu_m^{xz} \\ \mu_m^{yx} & \mu_m^{yy} & \mu_m^{yz} \\ \mu_m^{zx} & \mu_m^{zy} & \mu_m^{zz} \end{bmatrix} = \bar{\bar{\Xi}}_{H,m}^{-1} \cdot \begin{bmatrix} \mu_m^{(1)} & 0 & 0 \\ 0 & \mu_m^{(2)} & 0 \\ 0 & 0 & \mu_m^{(3)} \end{bmatrix} \cdot \bar{\bar{\Xi}}_{H,m} \tag{1b}$$

respectively, where $\epsilon_m^{(l)}$ and $\mu_m^{(l)}$ are the permittivity and permeability element aligned to the lth electric and magnetic principal axis of the mth scatterer, say $e_{E,m}^{(l)}$ and $e_{H,m}^{(l)}$ as indicated in Fig. 1, respectively, $l = 1, 2, 3$ and $m = 1, 2, \ldots, M$. Note that $\epsilon_m^{(l)} \neq \epsilon_0$ and $\mu_m^{(l)} \neq \mu_0$, where ϵ_0 and μ_0 are the permittivity and permeability of the background homogeneous medium, respectively, $l = 1, 2, 3$ and $m = 1, 2, \ldots, M$. The rotation transforming matrix $\bar{\bar{\Xi}}_{n,m}$ is the function of the rotation Euler angles $\phi_{n,m} \in [0, 2\pi], \theta_{n,m} \in [0, \pi]$ and $\varphi_{n,m} \in [0, 2\pi]$ [7], which are defined as the ones shown in Fig. 1, $n = E, H$ and $m = 1, 2, \ldots, M$.

For the M small spherical scatterers, we have $ka_m \ll 1$, where k is the wave number of the background medium, $m = 1, 2, \ldots, M$. Thus, by using the Foldy-Lax equation for small inclusions [4], [8], [9], [18], we could obtain the following relations between the total electric field $\bar{E}_t^{in}(\bar{r}_j)$ and magnetic field $\bar{H}_t^{in}(\bar{r}_j)$ incident upon the jth sphere

$$\begin{aligned} &\bar{E}_t^{in}(\bar{r}_j) \\ &\quad = \bar{E}_0^{in}(\bar{r}_j) + \sum_{m \neq j} \Big\{ i\omega\mu_0 \bar{\bar{G}}_0(\bar{r}_j, \bar{r}_m) \cdot \bar{\bar{\xi}}_m \cdot \bar{E}_t^{in}(\bar{r}_m) \\ &\qquad - \nabla g(\bar{r}_j, \bar{r}_m) \times \Big[\bar{\bar{\zeta}}_m \cdot \bar{H}_t^{in}(\bar{r}_m) \Big] \Big\} \end{aligned} \tag{2b}$$

$$\begin{aligned} &\bar{H}_t^{in}(\bar{r}_j) \\ &\quad = \bar{H}_0^{in}(\bar{r}_j) + \sum_{m \neq j} \Big\{ i\omega\epsilon_0 \bar{\bar{G}}_0(\bar{r}_j, \bar{r}_m) \cdot \bar{\bar{\zeta}}_m \cdot \bar{H}_t^{in}(\bar{r}_m) \\ &\qquad + \nabla g(\bar{r}_j, \bar{r}_m) \times \Big[\bar{\bar{\xi}}_m \cdot \bar{E}_t^{in}(\bar{r}_m) \Big] \Big\} \end{aligned} \tag{2b}$$

where $\bar{E}_0^{in}(\bar{r}_j)$ and $\bar{H}_0^{in}(\bar{r}_j)$ are the incident electric and magnetic fields excited by the antenna array at the position of jth scatterer, $j = 1, 2, \ldots, M, \bar{\bar{G}}_0(\bar{r}, \bar{r}^{'}) = (\bar{\bar{I}} + (\nabla\nabla/k^2)) g(\bar{r}, \bar{r}^{'})$ is the dyadic Green's function of the background medium and $g(\bar{r}, \bar{r}^{'}) = e^{ikR}/4\pi R$ with $R = |\bar{r} - \bar{r}^{'}|$, while

$$\begin{aligned} \bar{\bar{\xi}}_m &= -i4\pi k a_m^3 \sqrt{\frac{\epsilon_0}{\mu_0}} \bar{\bar{\Xi}}_{E,m}^{-1} \\ &\quad \cdot \mathtt{diag} \left[\frac{\epsilon_m^{(1)} - \epsilon_0}{\epsilon_m^{(1)} + 2\epsilon_0}, \frac{\epsilon_m^{(2)} - \epsilon_0}{\epsilon_m^{(2)} + 2\epsilon_0}, \frac{\epsilon_m^{(3)} - \epsilon_0}{\epsilon_m^{(3)} + 2\epsilon_0} \right] \cdot \bar{\bar{\Xi}}_{E,m} \end{aligned} \tag{3a}$$

and

$$\begin{aligned} \bar{\bar{\zeta}}_m &= -i4\pi k a_m^3 \sqrt{\frac{\mu_0}{\epsilon_0}} \bar{\bar{\Xi}}_{H,m}^{-1} \\ &\quad \cdot \mathrm{diag} \left[\frac{\mu_m^{(1)} - \mu_0}{\mu_m^{(1)} + 2\mu_0}, \frac{\mu_m^{(2)} - \mu_0}{\mu_m^{(2)} + 2\mu_0}, \frac{\mu_m^{(3)} - \mu_0}{\mu_m^{(3)} + 2\mu_0} \right] \cdot \bar{\bar{\Xi}}_{H,m} \end{aligned} \tag{3a}$$

are the electric and magnetic polarization strength tensors of the mth scatterer [10], respectively, $m = 1, 2, \ldots, M$.

Here we define a matrix operator $\bar{\bar{\chi}}(\bar{r}, \bar{r}^{'})$, so that $\bar{\bar{\chi}}(\bar{r}, \bar{r}^{'}) \cdot \bar{A} = \nabla g(\bar{r}, \bar{r}^{'}) \times \bar{A}$ for arbitrary vector $\bar{A}$ [11]. Then, (2a) and (2b) can be written in the matrix form

$$\bar{\bar{Q}} \cdot \bar{\bar{\Lambda}} \cdot \bar{\psi}_t^{in} = \bar{\psi}_0^{in} \tag{4}$$

where $\bar{\psi}_t^{in}$ and $\bar{\psi}_0^{in}$ are both $6M$-dimensional vectors

$$\begin{aligned} \bar{\psi}_t^{in} &= \big[\bar{E}_t^{in}(\bar{r}_1)^T, \bar{E}_t^{in}(\bar{r}_2)^T, \ldots, \bar{E}_t^{in}(\bar{r}_M)^T \\ &\qquad \bar{H}_t^{in}(\bar{r}_1)^T, \ldots, \bar{H}_t^{in}(\bar{r}_M)^T \big]^T \end{aligned} \tag{5a}$$

$$\begin{aligned} \bar{\psi}_0^{in} &= \big[\bar{E}_0^{in}(\bar{r}_1)^T, \bar{E}_0^{in}(\bar{r}_2)^T, \ldots, \bar{E}_0^{in}(\bar{r}_M)^T \\ &\qquad \bar{H}_0^{in}(\bar{r}_1)^T, \ldots, \bar{H}_0^{in}(\bar{r}_M)^T \big]^T \end{aligned} \tag{5b}$$

where the superscript T denotes the transpose, and both

$$\bar{\bar{\Lambda}} = \mathtt{diag}[\bar{\bar{\xi}}_1, \bar{\bar{\xi}}_2, \ldots, \bar{\bar{\xi}}_M, \bar{\bar{\zeta}}_1, \ldots, \bar{\bar{\zeta}}_M] \tag{6}$$

and

$$\bar{\bar{Q}} = \begin{bmatrix} \bar{\bar{\alpha}}, & \bar{\bar{\beta}} \\ -\bar{\bar{\beta}}, & \bar{\bar{\gamma}} \end{bmatrix} \tag{7}$$

are $6M$ by $6M$ matrices with (8a) to (8c), shown at the bottom of the following page. The scattered electric field at the position

of the qth antenna unit could be written as follows:

$$\bar{E}^s(\bar{r}_q^{'}) = \sum_{m=1}^{M} \Big\{ i\omega\mu_0 \bar{\bar{G}}_0(\bar{r}_q^{'}, \bar{r}_m) \cdot \bar{\bar{\xi}}_m \cdot \bar{E}_t^{in}(\bar{r}_m) - \nabla g(\bar{r}_q^{'}, \bar{r}_m) \times \Big[\bar{\bar{\zeta}}_m \cdot \bar{H}_t^{in}(\bar{r}_m) \Big] \Big\} \quad (9)$$

which leads to a linear equation system describing the scattered electric fields at the positions of all the antenna units

$$\bar{E}^s = \bar{\bar{\Omega}} \cdot \bar{\bar{\Lambda}} \cdot \bar{\psi}_t^{in} \quad (10)$$

where $\bar{E}^s = [\bar{E}^s(\bar{r}_1^{'})^T, \bar{E}^s(\bar{r}_2^{'})^T, \ldots, \bar{E}^s(\bar{r}_N^{'})^T]^T$ is a $3N$-dimensional vector, and $\bar{\bar{\Omega}} = [\bar{\bar{\mathbf{G}}}, -\bar{\bar{X}}]$ is a $3N$ by $6M$ matrix with (11a) and (11b), shown at the bottom of the page.

The incident fields at the positions of all scatterers, i.e., $\bar{\psi}_0^{in}$ in (4), are given by

$$\bar{\psi}_0^{in} = \begin{bmatrix} \bar{\bar{\mathbf{G}}}^T \\ \bar{\bar{\mathbf{X}}}^T \end{bmatrix} \cdot \bar{\bar{D}} \cdot \bar{I} = \bar{\bar{P}} \cdot \bar{\bar{D}} \cdot \bar{I} \quad (12)$$

where $\bar{\bar{D}} = \mathtt{diag}[d_{1x}, d_{1y}, d_{1z}, d_{2x}, d_{2y}, d_{2z}, \ldots, d_{Nz}]$ and $\bar{I} = [I_{1x}, I_{1y}, I_{1z}, I_{2x}, I_{2y}, I_{2z}, \ldots, I_{Nz}]^T$.

By using (10), (4), and (12), the voltage induced by the scattered fields at each component of the antenna array could be obtained via

$$\begin{aligned} \bar{V} &= \bar{\bar{D}} \cdot \bar{E}^s \\ &= \bar{\bar{D}} \cdot \bar{\bar{\Omega}} \cdot \bar{\bar{\Lambda}} \cdot \bar{\psi}_t^{in} \\ &= \bar{\bar{D}} \cdot \bar{\bar{\Omega}} \cdot \bar{\bar{Q}}^{-1} \bar{\psi}_0^{in} \\ &= \bar{\bar{D}} \cdot \bar{\bar{\Omega}} \cdot \bar{\bar{Q}}^{-1} \cdot \bar{\bar{P}} \cdot \bar{\bar{D}} \cdot \bar{I} \end{aligned} \quad (13)$$

where $\bar{V} = [V_{1x}, V_{1y}, V_{1z}, V_{2x}, V_{2y}, V_{2z}, \ldots, V_{Nz}]^T$. Thus, the multistatic response (MSR) matrix can be represented as

$$\bar{\bar{K}} = \bar{\bar{D}} \cdot \bar{\bar{\Omega}} \cdot \bar{\bar{Q}}^{-1} \cdot \bar{\bar{P}} \cdot \bar{\bar{D}}. \quad (14)$$

By reciprocity, we know that the MSR matrix $\bar{\bar{K}}$ is symmetric.

$$\bar{\bar{\alpha}} = \begin{bmatrix} \bar{\bar{\xi}}_1^{-1}, & -i\omega\mu_0\bar{\bar{G}}_0(\bar{r}_1,\bar{r}_2), & -i\omega\mu_0\bar{\bar{G}}_0(\bar{r}_1,\bar{r}_3), & \ldots, & -i\omega\mu_0\bar{\bar{G}}_0(\bar{r}_1,\bar{r}_M) \\ -i\omega\mu_0\bar{\bar{G}}_0(\bar{r}_2,\bar{r}_1), & \bar{\bar{\xi}}_2^{-1}, & -i\omega\mu_0\bar{\bar{G}}_0(\bar{r}_2,\bar{r}_3), & \ldots, & -i\omega\mu_0\bar{\bar{G}}_0(\bar{r}_2,\bar{r}_M) \\ -i\omega\mu_0\bar{\bar{G}}_0(\bar{r}_3,\bar{r}_1), & -i\omega\mu_0\bar{\bar{G}}_0(\bar{r}_3,\bar{r}_2), & \bar{\bar{\xi}}_3^{-1}, & \ldots, & -i\omega\mu_0\bar{\bar{G}}_0(\bar{r}_3,\bar{r}_M) \\ & \vdots & & \ddots & \vdots \\ -i\omega\mu_0\bar{\bar{G}}_0(\bar{r}_M,\bar{r}_1), & -i\omega\mu_0\bar{\bar{G}}_0(\bar{r}_M,\bar{r}_2), & -i\omega\mu_0\bar{\bar{G}}_0(\bar{r}_M,\bar{r}_3), & \ldots, & \bar{\bar{\xi}}_M^{-1} \end{bmatrix} \quad (8a)$$

$$\bar{\bar{\beta}} = \begin{bmatrix} \bar{\bar{0}}, & \bar{\bar{\chi}}(\bar{r}_1,\bar{r}_2), & \bar{\bar{\chi}}(\bar{r}_1,\bar{r}_3), & \ldots & \bar{\bar{\chi}}(\bar{r}_1,\bar{r}_M) \\ \bar{\bar{\chi}}(\bar{r}_2,\bar{r}_1), & \bar{\bar{0}}, & \bar{\bar{\chi}}(\bar{r}_2,\bar{r}_3), & \ldots & \bar{\bar{\chi}}(\bar{r}_2,\bar{r}_M) \\ \bar{\bar{\chi}}(\bar{r}_3,\bar{r}_1), & \bar{\bar{\chi}}(\bar{r}_3,\bar{r}_2), & \bar{\bar{0}}, & \ldots & \bar{\bar{\chi}}(\bar{r}_3,\bar{r}_M) \\ & \vdots & & \ddots & \vdots \\ \bar{\bar{\chi}}(\bar{r}_M,\bar{r}_1), & \bar{\bar{\chi}}(\bar{r}_M,\bar{r}_2), & \bar{\bar{\chi}}(\bar{r}_M,\bar{r}_3), & \ldots & \bar{\bar{0}} \end{bmatrix} \quad (8b)$$

and

$$\bar{\bar{\gamma}} = \begin{bmatrix} \bar{\bar{\zeta}}_1^{-1}, & -i\omega\epsilon_0\bar{\bar{G}}_0(\bar{r}_1,\bar{r}_2), & -i\omega\epsilon_0\bar{\bar{G}}_0(\bar{r}_1,\bar{r}_3), & \ldots, & -i\omega\epsilon_0\bar{\bar{G}}_0(\bar{r}_1,\bar{r}_M) \\ -i\omega\epsilon_0\bar{\bar{G}}_0(\bar{r}_2,\bar{r}_1), & \bar{\bar{\zeta}}_2^{-1}, & -i\omega\epsilon_0\bar{\bar{G}}_0(\bar{r}_2,\bar{r}_3), & \ldots, & -i\omega\epsilon_0\bar{\bar{G}}_0(\bar{r}_2,\bar{r}_M) \\ -i\omega\epsilon_0\bar{\bar{G}}_0(\bar{r}_3,\bar{r}_1), & -i\omega\epsilon_0\bar{\bar{G}}_0(\bar{r}_3,\bar{r}_2), & \bar{\bar{\zeta}}_3^{-1}, & \ldots, & -i\omega\epsilon_0\bar{\bar{G}}_0(\bar{r}_3,\bar{r}_M) \\ & \vdots & & \ddots & \vdots \\ -i\omega\epsilon_0\bar{\bar{G}}_0(\bar{r}_M,\bar{r}_1), & -i\omega\epsilon_0\bar{\bar{G}}_0(\bar{r}_M,\bar{r}_2), & -i\omega\epsilon_0\bar{\bar{G}}_0(\bar{r}_M,\bar{r}_3), & \ldots, & \bar{\bar{\zeta}}_M^{-1} \end{bmatrix}. \quad (8c)$$

$$\bar{\bar{\mathbf{G}}} = \begin{bmatrix} i\omega\mu_0\bar{\bar{G}}_0(\bar{r}_1^{'},\bar{r}_1), & i\omega\mu_0\bar{\bar{G}}_0(\bar{r}_1^{'},\bar{r}_2), & i\omega\mu_0\bar{\bar{G}}_0(\bar{r}_1^{'},\bar{r}_3), & \ldots, & i\omega\mu_0\bar{\bar{G}}_0(\bar{r}_1^{'},\bar{r}_M) \\ i\omega\mu_0\bar{\bar{G}}_0(\bar{r}_2^{'},\bar{r}_1), & i\omega\mu_0\bar{\bar{G}}_0(\bar{r}_2^{'},\bar{r}_2), & i\omega\mu_0\bar{\bar{G}}_0(\bar{r}_2^{'},\bar{r}_3), & \ldots, & i\omega\mu_0\bar{\bar{G}}_0(\bar{r}_2^{'},\bar{r}_M) \\ i\omega\mu_0\bar{\bar{G}}_0(\bar{r}_3^{'},\bar{r}_1), & i\omega\mu_0\bar{\bar{G}}_0(\bar{r}_3^{'},\bar{r}_2), & i\omega\mu_0\bar{\bar{G}}_0(\bar{r}_3^{'},\bar{r}_3), & \ldots, & i\omega\mu_0\bar{\bar{G}}_0(\bar{r}_3^{'},\bar{r}_M) \\ & \vdots & & \ddots & \vdots \\ i\omega\mu_0\bar{\bar{G}}_0(\bar{r}_N^{'},\bar{r}_1), & i\omega\mu_0\bar{\bar{G}}_0(\bar{r}_N^{'},\bar{r}_2), & i\omega\mu_0\bar{\bar{G}}_0(\bar{r}_N^{'},\bar{r}_3), & \ldots, & i\omega\mu_0\bar{\bar{G}}_0(\bar{r}_N^{'},\bar{r}_M) \end{bmatrix} \quad (11a)$$

and

$$\bar{\bar{\mathbf{X}}} = \begin{bmatrix} \bar{\bar{\chi}}(\bar{r}_1^{'},\bar{r}_1), & \bar{\bar{\chi}}(\bar{r}_1^{'},\bar{r}_2), & \bar{\bar{\chi}}(\bar{r}_1^{'},\bar{r}_3), & \ldots & \bar{\bar{\chi}}(\bar{r}_1^{'},\bar{r}_M) \\ \bar{\bar{\chi}}(\bar{r}_2^{'},\bar{r}_1), & \bar{\bar{\chi}}(\bar{r}_2^{'},\bar{r}_2), & \bar{\bar{\chi}}(\bar{r}_2^{'},\bar{r}_3), & \ldots & \bar{\bar{\chi}}(\bar{r}_2^{'},\bar{r}_M) \\ \bar{\bar{\chi}}(\bar{r}_3^{'},\bar{r}_1), & \bar{\bar{\chi}}(\bar{r}_3^{'},\bar{r}_2), & \bar{\bar{\chi}}(\bar{r}_3^{'},\bar{r}_3), & \ldots & \bar{\bar{\chi}}(\bar{r}_3^{'},\bar{r}_M) \\ & \vdots & & \ddots & \vdots \\ \bar{\bar{\chi}}(\bar{r}_N^{'},\bar{r}_1), & \bar{\bar{\chi}}(\bar{r}_N^{'},\bar{r}_2), & \bar{\bar{\chi}}(\bar{r}_N^{'},\bar{r}_3), & \ldots & \bar{\bar{\chi}}(\bar{r}_N^{'},\bar{r}_M) \end{bmatrix}. \quad (11b)$$

III. Inverse Scattering Problem

A. The Implementation of the Music Algorithm for Estimating the Positions of the Scatterers

For point-like targets, the MUSIC algorithm has been proved to be applicable in acoustics [4], which shows that the range space of the MSR matrix is spanned by the background Green's function vectors evaluated at the scatterer locations. For the electromagnetic case, however, the background Green's function is a dyadic function. From the expression of MSR matrix in (14), we find that, for the small anisotropic spheres whose principle elements of the permittivity and permeability tensors are different from those of the background homogeneous medium, if $6M < 3N$, the rank of the $3N$ by $3N$ MSR matrix is $6M$, and the range space of the MSR matrix is spanned by the background Green's function vectors corresponding to the x, y and z components of the electric and magnetic dipoles induced in each scatterer, i.e., $S_r = \mathtt{Span}\{\bar{\bar{\mathbf{G}}}_x(\bar{r}_i), \bar{\bar{\mathbf{G}}}_y(\bar{r}_i), \bar{\bar{\mathbf{G}}}_z(\bar{r}_i), \bar{\bar{\mathbf{X}}}_x(\bar{r}_i), \bar{\bar{\mathbf{X}}}_y(\bar{r}_i), \bar{\bar{\mathbf{X}}}_z(\bar{r}_i); i = 1, 2, \ldots, M\}$, where $\bar{\bar{\mathbf{G}}}_x(\bar{r}_i), \bar{\bar{\mathbf{G}}}_y(\bar{r}_i)$ and $\bar{\bar{\mathbf{G}}}_z(\bar{r}_i)$ are the $[3(i-1)+1]^{\text{th}}$, $[3(i-1)+2]^{\text{th}}$, and $[3(i-1)+3]^{\text{th}}$ column of matrix $\bar{\bar{\mathbf{G}}}$, respectively, and $\bar{\bar{\mathbf{X}}}_x(\bar{r}_i), \bar{\bar{\mathbf{X}}}_y(\bar{r}_i)$ and $\bar{\bar{\mathbf{X}}}_z(\bar{r}_i)$ the $[3(i-1)+1]^{\text{th}}$, $[3(i-1)+2]^{\text{th}}$, and $[3(i-1)+3]^{\text{th}}$ column of matrix $\bar{\bar{\mathbf{X}}}$, respectively. This is similar to the analysis of the time-reversal operator in [12] and is due to the fact that, for small anisotropic spheres whose principle elements of the permittivity and permeability tensors are different from those of the background medium, the x, y and z directions' electric and magnetic dipoles could be excited independently in each scatterer. Thus, the total $6M$ background Green's function vectors, $\bar{\bar{\mathbf{G}}}_x(\bar{r}_i), \bar{\bar{\mathbf{G}}}_y(\bar{r}_i), \bar{\bar{\mathbf{G}}}_z(\bar{r}_i), \bar{\bar{\mathbf{X}}}_x(\bar{r}_i), \bar{\bar{\mathbf{X}}}_y(\bar{r}_i)$ and $\bar{\bar{\mathbf{X}}}_z(\bar{r}_i), i = 1, 2, \ldots, M$, are linearly independent. From the singular value decomposition analysis [13], the MSR matrix could be represented as $\bar{\bar{K}} \cdot \bar{v}_p = \sigma_p \bar{u}_p$ and $\bar{\bar{K}}^* \cdot \bar{u}_p = \sigma_p \bar{v}_p$, where the superscript $*$ denotes the Hermitian, so that the left null space of the MSR matrix is $S_n = \mathtt{Span}\{\bar{u}_p; \sigma_p = 0\}$. Due to the orthogonality between the range space S_r and the left null space S_n, we have $|\bar{u}_p^* \bar{\bar{\mathbf{G}}}_l(\bar{r}_m)| = 0$ and $|\bar{u}_p^* \bar{\bar{\mathbf{X}}}_l(\bar{r}_m)| = 0$, for $\sigma_p = 0, m = 1, 2, \ldots, M$ and $l = x, y, z$. Following the manner defined by Devaney *et al.* [4], as long as $6M < 3N$, the MUSIC pseudo-spectrum is

$$\Phi(\bar{r}) = \frac{1}{\sum_{\sigma_p=0} \left[\sum_{l=x,y,z} \left| \bar{u}_p^* \bar{\bar{\mathbf{G}}}_l(\bar{r}) \right|^2 + \sum_{l=x,y,z} \left| \bar{u}_p^* \bar{\bar{\mathbf{X}}}_l(\bar{r}) \right|^2 \right]} \tag{15}$$

which becomes infinite at the position of each scatterer. In order to locate M targets, the number of antenna units could be chosen as the minimum integer N that satisfies $6M < 3N$. In practice, more antenna units have to be used due to the presence of noise. The number of antenna units actually used depends on various factors, such as the separation between targets, the polarization strength tensors of targets, distances between antennas and targets, and the level of noise.

B. The Non-Iterative Analytical Method for Retrieving the Polarization Strength Tensors

After estimating the positions of the scatterers, we need to retrieve the polarization strength tensors of each scatterer, and this is a nonlinear problem considering the multiple scattering effect (MSE). However, instead of using the iterative method proposed in [4], one can solve such a nonlinear problem through linear approaches used in acoustics [14] and [15]. In [14], in order to obtain the scattering strength of a scatterer, the fact that the background Green's function vectors are linearly independent is used to generate M equations. One of these equations, referred to as the prime equation hereafter, is used to solve for the scattering strength whereas the other $M-1$ equations act as constraints. In the absence of noise, the $M-1$ constraints are satisfied and the solved scattering strength is exact. However, in the presence of noise, these constraints are violated and solving for the scattering strength from the prime equation alone results in relatively large error. In comparison, the method in [15] does not have constraint equations and uses least squares method twice to minimize errors of the estimates of scattering strengths, which is shown to be more robust than the method presented in [14] in the presence of noise [15]. Here we apply the method in [15] to the present electromagnetic problem. First, taking $\bar{\bar{Q}}^{-1} \cdot \bar{\bar{P}}$ as unknowns in (14), one obtains its least squares solution given by

$$\bar{\bar{Q}}^{-1} \cdot \bar{\bar{P}} = \bar{\bar{\Omega}}^{\dagger} \cdot \tilde{\bar{K}} \tag{16}$$

where $\tilde{\bar{K}} = \bar{\bar{D}}^{-1} \cdot \bar{\bar{K}} \cdot \bar{\bar{D}}^{-1}$. Then, we split matrix $\bar{\bar{Q}}$ into two parts, say $\bar{\bar{Q}}_1$ and $\bar{\bar{Q}}_2$, where

$$\bar{\bar{Q}}_1 = \mathtt{diag}\left[\bar{\bar{\xi}}_1^{-1}, \bar{\bar{\xi}}_2^{-1}, \ldots, \bar{\bar{\xi}}_M^{-1}, \bar{\bar{\zeta}}_1^{-1}, \ldots, \bar{\bar{\zeta}}_M^{-1} \right] \tag{17}$$

and $\bar{\bar{Q}}_2 = \bar{\bar{Q}} - \bar{\bar{Q}}_1$.

After estimating the positions of the scatterers, the matrices $\bar{\bar{\Omega}}$, $\bar{\bar{P}}$ and $\bar{\bar{Q}}_2$ are known, and the unknown polarization strength tensors $\bar{\bar{\xi}}_m$ and $\bar{\bar{\zeta}}_m$ are embedded in $\bar{\bar{Q}}_1$. From (16), we have an equation for $\bar{\bar{Q}}_1$

$$\bar{\bar{Y}} \cdot \bar{\bar{Q}}_1^T = \bar{\bar{Z}} \tag{18}$$

where $\bar{\bar{Y}} = (\bar{\bar{\Omega}}^{\dagger} \cdot \tilde{\bar{K}})^T$ and $\bar{\bar{Z}} = [\bar{\bar{P}} - \bar{\bar{Q}}_2 \cdot \bar{\bar{\Omega}}^{\dagger} \cdot \tilde{\bar{K}}]^T$ with $\dagger$ denoting the psuedoinverse operator [13]. Thus, the polarization strength tensors could be obtained by the least squares method as

$$\bar{\bar{\xi}}_m = \left[(\bar{\bar{Y}}_m^{\dagger} \cdot \bar{\bar{Z}}_m)^T \right]^{-1} \tag{19a}$$

and

$$\bar{\bar{\zeta}}_m = \left[(\bar{\bar{Y}}_{M+m}^{\dagger} \cdot \bar{\bar{Z}}_{M+m})^T \right]^{-1} \tag{19b}$$

$m = 1, 2, \ldots, M$. Here, matrices $\bar{\bar{Y}}_j$ and $\bar{\bar{Z}}_j$ are defined as $\bar{\bar{Y}}_j = [\bar{Y}_{3(j-1)+1}, \bar{Y}_{3(j-1)+2}, \bar{Y}_{3(j-1)+3}]$, and $\bar{\bar{Z}}_j = [\bar{Z}_{3(j-1)+1}, \bar{Z}_{3(j-1)+2}, \bar{Z}_{3(j-1)+3}]$, where $\bar{Y}_i$ and $\bar{Z}_i$ are the ith column of matrices $\bar{\bar{Y}}$ and $\bar{\bar{Z}}$, respectively, $j = 1, 2, \ldots, 2M$, and $i = 1, 2, \ldots, 6M$. Note that the solutions given by (19a) and (19b) are exact for the noise-free situation, and are the least squares solutions in the presence of noise.

In order to obtain the transforming tensors $\bar{\bar{\Xi}}_{E,m}$ and $\bar{\bar{\Xi}}_{H,m}$ for the mth scatterer, which tell the orientations of the electric and magnetic principal axes of the scatterers, we apply the

eigenvalue decomposition to the polarization strength tensor $\bar{\bar{\xi}}_m$ and $\bar{\bar{\zeta}}_m$, respectively, and (3a) and (3b) show that the resulting eigenvectors give the information of transforming tensors $\bar{\bar{\bar{\Xi}}}_{E,m}$ and $\bar{\bar{\bar{\Xi}}}_{H,m}, m = 1, 2, \ldots, M$.

The above derivation is for the case where the MSE is considered. When the MSE is ignored, we let $\bar{\bar{Z}} = \bar{\bar{P}}^T$ and follow the same aforementioned procedure. Note that when the MSE is ignored, the Foldy-Lax equation reduces to distorted Born approximation.

In deriving the MSR matrix $\bar{\bar{K}}$, we assume that mutual coupling between antennas could be totally eliminated. However, in practice, measurement system has to be carefully set up to reduce mutual coupling effect. If the measurement error of the MSR matrix were large due to mutual coupling, algorithms for the inverse scattering problem would not work properly. However, mutual coupling effect could be possibly circumvented by some methods, such as using other kind of transmitter and receiver. If so, the matrix $\bar{\bar{P}} \cdot \bar{\bar{D}}$ in (14) is replaced by another matrix determined by the Green's functions of the transmitter and the left most $\bar{\bar{D}}$ matrix in (14) is removed if scattered field instead of induced voltage is measured in the receiver. But it is easy to see that these changes will not affect the essence of our inversion algorithm.

IV. Numerical Simulations

Two numerical simulations are presented in this section to test the proposed inversion methods. The first one deals with the far-field imaging and retrieval of the polarization strength tensors of two well-separated targets, and the second one is for the near-field imaging and retrieval of the polarization strength tensors of four targets close to each other. Both of the two simulations were carried out under the assumption that the scattering data are contaminated with noise. We first calculated the forward problem to give the MSR matrix $\bar{\bar{K}}$ by using (14), and then we added the additive white Gaussian noise to the MSR matrix. The noise level is quantified by the signal to noise ratio (SNR) in dB defined as $20\log_{10}(\|\bar{\bar{K}}\|)/(\|\bar{\bar{\kappa}}\|)$, where $\bar{\bar{\kappa}}$ is the additive white Gaussian noise and $\|\cdot\|$ denotes the Frobenius norm of a matrix [4]. In the numerical simulations, the MSR matrix is the arithmetic mean of 10 noisy MSR matrices. Such a procedure simulates a practical operation in which the MSR matrix is given by an arithmetical average of 10 measurements.

After applying the non-iterative retrieval method described in Section III, we obtain the electric and magnetic polarization strength tensors estimates, $\bar{\bar{\xi}}_m^{'}$ and $\bar{\bar{\zeta}}_m^{'}, m = 1, 2, \ldots, M$. The accuracy of the estimation of the polarization strength tensors was quantified by a normalized percent error as follows:

$$E = \sum_{m=1}^{M} \frac{\sum_{i=1}^{3}\sum_{j=1}^{3} |\bar{\bar{\xi}}_{m,ij}^{'} - \bar{\bar{\xi}}_{m,ij}|^2}{\sum_{i=1}^{3}\sum_{j=1}^{3} |\bar{\bar{\xi}}_{m,ij}|^2} \times 100\% \qquad (20)$$

where $\bar{\bar{\xi}}_{m,ij}^{'}$ is the element of the estimated electric polarization strength tensor $\bar{\bar{\xi}}_m^{'}$ (or the estimated magnetic polarization strength tensor $\bar{\bar{\zeta}}_m^{'}$), and $\bar{\bar{\xi}}_{m,ij}$ is the actual element of the electric polarization strength tensor $\bar{\bar{\xi}}_m$ (or the magnetic polarization strength tensor $\bar{\bar{\zeta}}_m$), $m = 1, 2, \ldots, M$.

In the following two simulations, all the orientations of the principle axes of each scatterer are generated randomly. The frequency of the electromagnetic wave was set to be $f = 100$ MHz. Each antenna unit used in the simulations has three antenna orientated in x, y, and z direction with the same length $d_{ix} = d_{iy} = d_{iz} = \lambda/50, i = 1, 2, \ldots, N$, where λ is the wavelength in vacuum of the electromagnetic wave at frequency $f = 100$ MHz.

A. Imaging and Retrieval of the Polarization Strength Tensors of the Well-Separated Spheres

In the first numerical simulation, the total of two scatterers with the same radius $a_m = \lambda/30$ were placed in the $z = 0$ plane with the x and y coordinates (0,0), and $(0, \lambda)$, and the principle elements of the permittivity and permeability tensors were set to be

$$\begin{cases} \epsilon_m^{(1)} = [3 + (-1)^m]\epsilon_0 \\ \epsilon_m^{(2)} = [4 + 0.5(-1)^{m+1}]\epsilon_0 \\ \epsilon_m^{(3)} = [5 + 0.25(-1)^m]\epsilon_0 \end{cases}$$
$$\begin{cases} \mu_m^{(1)} = [2 + 0.5(-1)^m]\mu_0 \\ \mu_m^{(2)} = [2.5 + 0.25(-1)^m]\mu_0 \\ \mu_m^{(3)} = [3 + 0.75(-1)^{m+1}]\mu_0 \end{cases} \qquad (21)$$

$m = 1, 2$. The orientation of the electric and magnetic principle axes were randomly chosen.

There were 16 antenna units employed in this simulation, half of which were aligned along the x axis while the other half aligned along the y axis in the $z = 10\lambda$ plane. The two linear arrays were centered directly above the origin of the coordinate system with 5λ separation distance between neighboring units. The simulation was carried out under the SNR from 15 dB to 30 dB. The normalized pseudo-spectrum in $z = 0$ plane at 15 dB SNR is shown in Fig. 2(a), which shows that the MUSIC algorithm could give a good estimation of the positions of the scatterers even though the SNR is low. After reading the positions from the pseudo-spectrum image, the non-iterative analytical method was applied to retrieve the polarization tensors, and results are shown in Fig. 2(b) for the SNR from 15 dB to 30 dB. In Fig. 2(b), although the inaccuracy of the estimation of the polarization tensors mainly decreases as the SNR increases, there are some fluctuations. Since the non-iterative retrieval method depends on the measured MSR matrix and the positions of the scatterers, the inaccuracy of the final estimations is caused by the noise contained in the MSR matrix and the errors in the estimation of the positions. We attribute the fluctuations in Fig. 2(b) mainly to the errors in the estimation of the positions. To verify this, we further assume that the correct positions of all the scatterers are already known ($\bar{\bar{Q}}_2$, $\bar{\bar{P}}$, and $\bar{\bar{\Omega}}$ are chosen to be the actual values), and the result excluding the position errors is shown in Fig. 2(c). Comparing the results shown in Fig. 2(b) and (c), we clearly see that, after excluding the position errors, the errors of the estimation of the polarization tensors are much smaller and the fluctuations are also much smaller, which is due to the noise in the MSR matrix. Such a correlation between the position errors and the errors of the estimations of the polarization tensors has also been mentioned by Devaney *et al.* in [4].

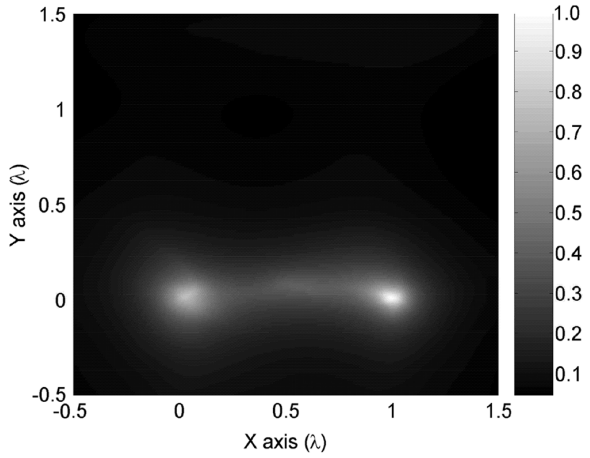

(a)

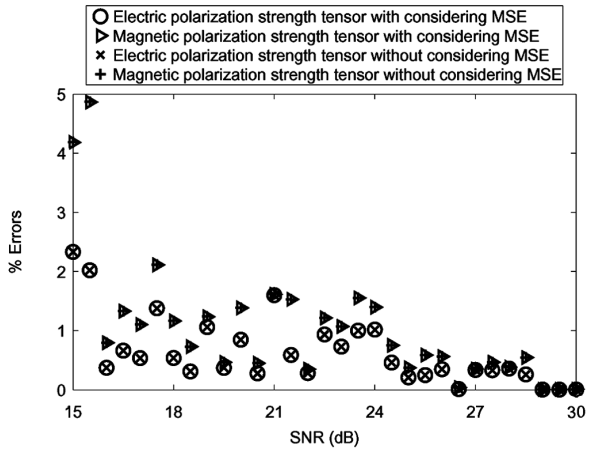

(b)

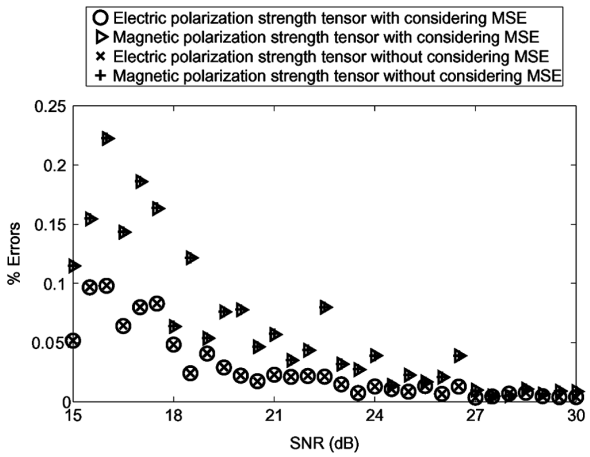

(c)

Fig. 2. Pseudo-spectrum image and the accuracy of the retrieval of the polarization strength tensors for two small anisotropic spheres located at (0,0) and $(0, \lambda)$. (a) The normalized pseudo-spectrum in $z = 0$ plane at 15 dB SNR.. (b) The percentage errors of the estimations of the polarization strength tensors when the position errors are included. (c) The percentage errors of the estimations of the polarization strength tensors when the position errors are excluded.

Furthermore, as we expected, there is no appreciable difference between the results obtained by the non-iterative analytical retrieval method with and without considering the MSE, since the separation between the two small spheres is far enough.

B. Imaging and Retrieval of the Polarization Strength Tensors of the Closely-Separated Spheres

In our second numerical simulation, the total of four scatterers with same radius $a_m = \lambda/30$ were placed in the $z = 0$ plane with the x and y coordinates (0,0), $(0, \lambda/12), (\lambda/12, 0)$ and $(\lambda/12, \lambda/12)$, and the permittivity and permeability elements along the principle axes were set to be

$$\begin{cases} \epsilon_m^{(1)} = [3 + (-1)^m + 0.1m]\epsilon_0 \\ \epsilon_m^{(2)} = [4 + 0.5(-1)^{m+1} + 0.1m]\epsilon_0 \\ \epsilon_m^{(3)} = [5 + 0.25(-1)^m + 0.1m]\epsilon_0 \end{cases}$$
$$\begin{cases} \mu_m^{(1)} = [2 + 0.5(-1)^m + 0.1m]\mu_0 \\ \mu_m^{(2)} = [2.5 + 0.25(-1)^m + 0.1m]\mu_0 \\ \mu_m^{(3)} = [3 + 0.75(-1)^{m+1} + 0.1m]\mu_0 \end{cases} \quad (22)$$

$m = 1, 2, 3, 4$. The orientation of the electric and magnetic principle axes were randomly chosen.

There were 45 antenna units employed in this simulation which were located in three circles. The three circles, whose centers were at the origin and radii were $\lambda/3$, were placed in xy, yz and xz plane, respectively, with 15 antenna units uniformly distributed along the perimeter of each. The simulation was taken under the SNR from 40 dB to 55 dB. The normalized pseudo-spectrum in $z = 0$ plane at 40 dB SNR is shown in Fig. 3, from which we see that the MUSIC method obtains a good estimation of the position of each scatterer. The estimations errors of the electric and magnetic polarization strength tensors including the position errors (position data are read from the image data) and excluding the position errors (assuming that the correct positions of all scatterer are known) are shown in Fig. 3(b) and (c), respectively. Different from the results in the previous simulation for the well-separated spheres, either including or excluding the position errors, the accuracy of the estimations of the polarization strength tensors was improved obviously by considering the MSE, indicating that the multiple scattering between closely spaced spheres cannot be ignored in this case. Furthermore, comparing these two results, we also conclude that the high percentage errors of the estimations at low SNR is mainly contributed by the inaccuracy of the position estimations. Finally, Fig. 3(c) shows that the estimation error for the electric polarization strength tensor is larger than that of the magnetic polarization strength tensor. This can be explained by (22), where we see the magnitudes of relative permittivities are larger than those of relative permeabilities. Thus induced electric dipoles and the electric fields produced by them play more roles in multiple scattering than their magnetic counterparts. Therefore, if MSE is ignored, more portion of electric field than magnetic field is neglected, resulting in more error in the estimation of electric polarization strength.

V. Conclusion

By using the Foldy-Lax equation, we proposed a multiple scattering model for the multiple-scattering small anisotropic spheres in this paper. We find that, for the small anisotropic spheres whose principle elements of the permittivity and permeability tensors are different from the permittivity and

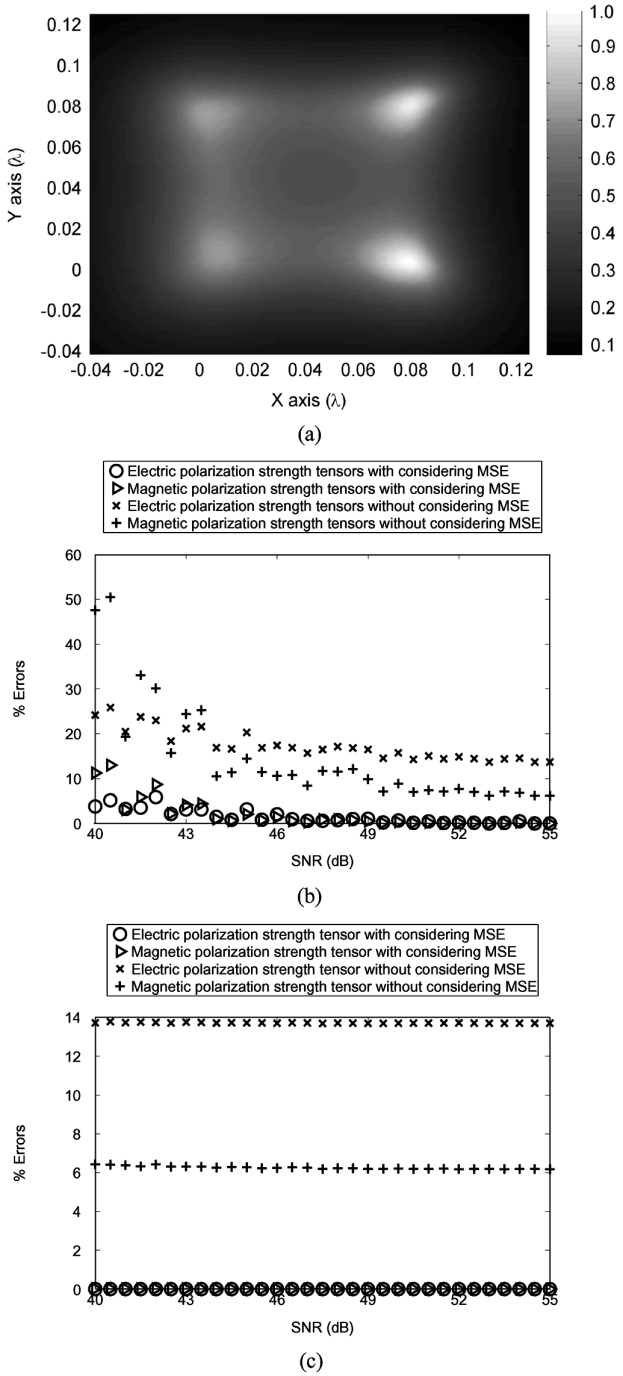

Fig. 3. Pseudo-spectrum image and the accuracy of the retrieval of the polarization strength tensors for four small anisotropic spheres located at (0,0), $(0, \lambda/12)$, $(\lambda/12, 0)$ and $(\lambda/12, \lambda/12)$. (a) The normalized pseudo-spectrum in $z = 0$ plane at 40 dB SNR. (b) The percentage errors of the estimations of the polarization strength tensors when the position errors are included. (c) The percentage errors of the estimations of the polarization strength tensors when the position errors are excluded.

permeability of the background homogeneous medium, respectively, if the number of the non-zero singular values of the MSR matrix is smaller than the number of the antennas, i.e., $6M < 3N$, the range of the MSR matrix is spanned by the total $6M$ background Green's function vectors corresponding to the x, y and z component of the electric and magnetic dipoles induced in each scatterer. Therefore, the MUSIC algorithm could be implemented to locate the small anisotropic spherical scatterers based on this model. After estimating the positions of the scatterers, we propose a non-iterative analytical method to retrieve the polarization strength tensors as well as the orientations of the principle axes of each scatterer. Two numerical experiments show that, the MUSIC algorithm could obtain a good estimation of the positions of the scatterers both well-separated and closely-separated, and the non-iterative analytical retrieval method obtains a better result after considering the MSE between the closely distributed scatterers. Thus, the nonlinear inverse scattering problem for the multiple-scattering small anisotropic spheres is solved by using two non-iterative methods: the MUSIC algorithm to locate the scatterers, and the non-iterative analytical retrieval method to obtain the polarization strength tensors as well as the orientations of the principle axes of each scatterer. The methods presented in this paper could also be applied to the inversion of the small isotropic spheres or the small bianisotropic spheres by substituting the elements in the polarization strength tensors with the ones shown in [10] and [16], respectively.

ACKNOWLEDGMENT

X. Chen would like to thank D. H. Chambers for bringing [6] to attention.

REFERENCES

[1] A. J. Devaney, "Time reversal imaging of obscured targets from multistatic data," *IEEE Trans. Antennas Propag.*, vol. 53, no. 5, pp. 1600–1610, 2005.

[2] C. Prada and M. Fink, "Eigenmodes of the time reversal operator: A solution to selective focusing in multiple-target media," *Wave Motion*, vol. 20, pp. 151–163, 1994.

[3] G. Micolau, M. Saillard, and P. Borderies, "DORT method as applied to Ultrawideband signals for detection of buried objects," *IEEE Trans. Geosci. Remote Sensing*, vol. 41, no. 8, pp. 1813–1820, Aug. 2003.

[4] A. J. Devaney, E. A. Marengo, and F. K. Gruber, "Time-reversal-based imaging and inverse scattering of multiply scattering point targets," *J. Acoust. Soc. Am.*, vol. 118, pp. 3129–3138, 2005.

[5] M. Cheney, "The linear sampling method and the MUSIC algorithm," *Inverse Problem*, vol. 17, pp. 591–595, 2001.

[6] H. Ammari, E. Iakovleva, D. Lesselier, and G. Perruson, "MUSIC-type electromagnetic imaging of a collection of small three-dimensional bounded inclusions," *SIAM Sci. Comput.*, vol. 29, pp. 674–709, 2007.

[7] G. B. Arfken and H. J. Weber, *Mathematical Methods for Physicists*, 5th ed. San Diego, CA: (Harcourt/Academic Press, 2001.

[8] J. H. Bruning and Y. T. Lo, "Multiple scattering of EM waves by spheres Part I—Multipole expansion and ray-optical solutions," *IEEE Trans. Antennas Propag.*, vol. 19, no. 3, pp. 378–390, May 1971.

[9] L. Tsang, J. A. Kong, K.-H. Ding, and C. O. Ao, *Scattering of Electromagnetic Waves: Numerical Simulations*. New York: Wiley-Interscience, 2001.

[10] C. F. Bohren and D. R. Huffman, *Absorption and Scattering of Light by Small Particles*. New York: Wiley, 1998.

[11] J. A. Kong, *Electromagnetic Wave Theory*. New York: EMW Publishing, 2005.

[12] D. H. Chambers and J. G. Berryman, "Analysis of the time-reversal operator for a small spherical scatterer in an electromagnetic field," *IEEE Trans. Antennas Propag.*, vol. 52, no. 7, pp. 1729–1738, Jul. 2004.

[13] R. A. Horn and C. R. Johnson, *Matrix Analysis*. Cambridge, U.K.: Cambridge Univ. Press, 1986.

[14] E. A. Marengo and F. K. Gruber, "Noniterative analytical formula for inverse scattering of multiply scattering point targets," *J. Acoust. Soc. Am.*, vol. 120, pp. 3782–3788, 2006.

[15] X. Chen and Y. Zhong, "A robust noniterative method for obtaining scattering strengths of multiply scattering point targets," *J. Acoust. Soc. Am.*, vol. 122, pp. 1325–1327, 2007.

[16] I. V. Lindell, A. H. Sihvola, S. A. Tretyakov, and A. J. Viitanen, *Electromagnetic Waves in Chiral and Bi-Isotropic Media*. Norwood, MA: Artech House, 1994.

[17] A. Kirsch, "The MUSIC-algorithm and the factorization method in inverse scattering theory for inhomogeneous media," *Inverse Problems*, vol. 18, pp. 1025–1040, 2002.
[18] M. Lax, "Multiple scattering of waves," *Reviews Modern Phys.*, vol. 23, pp. 287–310, 1951.

Yu Zhong received the B.S. and M.S. degrees in electronic engineering from Zhejiang University, Hangzhou, China, in 2003 and 2006, respectively.

He is currently working toward the Ph.D. degree in the Department of Electrical and Computer Engineering at the National University of Singapore, Singapore, where he is as a Research scholar . His current research interests are mainly electromagnetic inverse problems.

Xudong Chen received the B.S. and M.S. degrees in electrical engineering from Zhejiang University, Hangzhou, China, in 1999 and 2001, respectively, and the Ph.D. degree from the Massachusetts Institute of Technology, Cambridge, in 2005.

He is currently an Assistant Professor in the Department of Electrical and Computer Engineering at the National University of Singapore. His research interests are mainly electromagnetic inverse problems.